Self-Consistent Approaches and Strain Heterogeneities in Two-Phase Elastoplastic Materials

Michel Bornert, Eveline Hervé, Claude Stolz, André Zaoui

Self-consistent approaches and strain heterogeneities in two-phase elastoplastic materials

Michel Bornert, Eveline Hervé, Claude Stolz, and André Zaoui

Laboratoire de Mécanique des Solides, CNRS URA 317,
Ecole Polytechnique, 91128 Palaiseau Cedex, France

The Generalized Self Consistent Scheme [GSCS] extended to the nonlinear case with help of a deformation theory of elastoplasticity is used to predict the strain heterogeneities that spread out in two phase elastoplastic materials submitted to a monotonic uniaxial load. Materials with different microstructural morphologies are considered. The single composite inclusion of the GSCS is an accurate representation of "matrix/inclusion" microstructures but it does not give a sufficient representation of the considered morphologies. That's why this model is extended to more general cases by using two or even more different spherical composite inclusions: local concentration fluctuations and local morphological inversions can then be modeled. The nonlinear extension is also modified: the composite inclusions are discretized into several concentric layers in order to take into better account the strain gradient along the radius and a new definition of the work-hardening parameter of each of these layers is proposed. The elastoplastic strain field in the single composite inclusion is also computed numerically by means of finite element methods and compared to the analytical result. Unfortunately, these modifications do not basically modify the strain heterogeneity predictions of the GSCS, which widely underestimate the measured strain heterogeneities in most of the cases. In fact, the inaccuracy of the GSCS in these cases is basically due to the appearance of long range shear bands that cannot be described by a local self-consistent approach.

INTRODUCTION

Recent work (Allais [1], Allais et al. [2]) has shown a severe discrepancy between experimental measurements of strain heterogeneities which spread out in two-phase elastoplastic materials submitted to a monotonic uniaxial load and predictions of the Generalized Self Consistent Scheme [GSCS] (Christensen and Lo [3]), extended to the nonlinear case by means of the deformation theory for elastoplasticity (Hervé and Zaoui [4]). This work was based on iron/silver blends, manufactured with powder metallurgy techniques. Several materials, with different iron volume fractions and different microstructural morphologies have been tested.

These materials have basically been separated into two morphological classes: the materials with a "matrix/inclusion" microstructure, in the configuration "iron in silver", referred to as "MI materials" in the following, and the materials with bi-continuous phases, referred to as "BC materials". This classification was based on morphological analysis, informations related to the elaboration techniques and confrontation between measured elastic constants and computed ones. In particular, the shear moduli predicted by the GSCS in the "iron in silver" configuration were consistent with the measured values for the MI materials. The BC materials were perceptibly stiffer.

It has been experimentally shown that the macroscopic elastoplastic tensile test curves were not very sensitive to the morphology. The curves computed with both configurations of the GSCS using the curves of the pure materials and the phase volume fraction are also very close and in good accordance with the experimental results. Figure 1 gives typical tensile test curves of such materials.

The elastoplastic behavior of these materials has also been characterized at the micro-scale with help of a special device which allows to measure components of the local strain field over a domain representative of the microstructure. The component along the tensile axis of the strain tensor has especially been studied: its average value over both phases has been computed and its distribution in each phase has been characterized by means of bar graphs. These quantities have been compared to their corresponding value given by the GSCS: the local field computed in the composite inclusion may indeed be compared to the local field in the material in a sense that will be stated more precisely later on.

The experimental results show an effect of the morphology on the strain distribution: for the same iron volume frac-

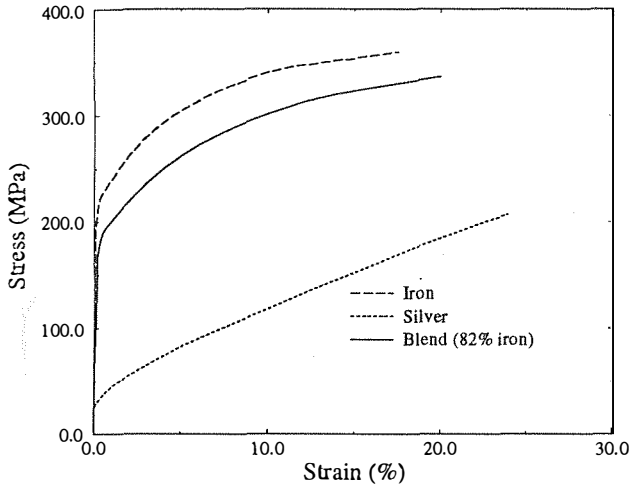

FIG 1. Macroscopic tensile tests

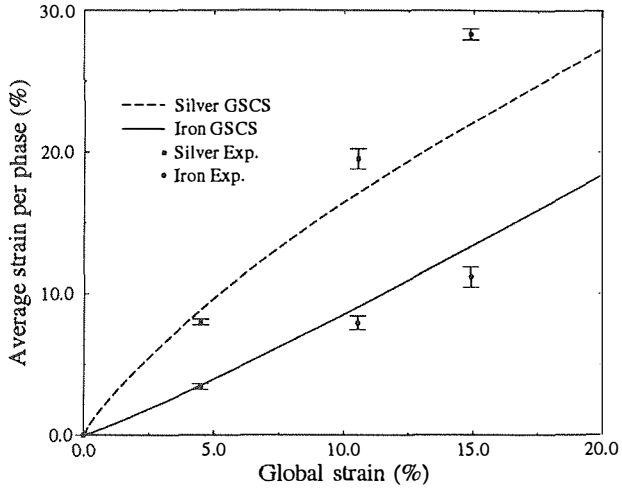

FIG 2. Average strain per phase

tion, the strain distribution may be different in two samples which have different microstructural morphologies: the average strains in both phases may be more or less close to each other and the strain distribution may be more or less wide. The results of the GSCS also show morphological effects: for identical local behaviors of the phases and the same volume fractions, the average strains in the phases are closer to each other in the configuration "silver in iron" than in the reverse one, and the strain distribution is wider in iron and narrower in silver.

The comparison between experimental results for MI materials and the values computed with the corresponding configuration of the GSCS leads to the following conclusions:

- At low global strain values (less than 5%), there is a satisfying accordance between experimental measurements and computed values of the average strain in both phases.
- At higher global strain values, the computed values of the average strains underestimate the observed interphase heterogeneities.
- The GSCS gives a satisfying information on the strain distribution in the silver phase (the matrix) for low global strain values (5%) and high iron phase concentration (75% and more).
- The width of the strain distribution predicted by the model in the silver phase is two to five times lower than the measured one, in all other cases.
- The strain distribution in the iron (the inclusion phase) is always underestimated by the model, whatever the phase concentration and the global strain are; the ratio between the width of the computed distribution and the measured one goes from five to more than ten.

Figures 2 to 6 sum up these results. Figure 2 gives the average strain in each phase as a function of the global strain. Figures 3 to 6 compare the experimental strain distribution functions to the computed ones, for both phases and at 5% and 15% global strain. All these results correspond to an MI sample with 82% iron and the local phase behaviors given in figure 1.

Even if the GSCS is not expected to represent correctly BC microstructures, one may also compare its predictions, in both configurations, to the experimental results obtained for BC materials. The above conclusions apply also to this case, except for the following points:

- The experimental average strains per phase are bounded by the values given by both configurations of the GSCS for low global strain values (5%). This is consistent with the elastic results: the shear moduli of the BC material lay somewhere between the predictions of both configurations of the GSCS.
- For higher global strain values (10% and 15%), both configurations underestimate the observed interphase heterogeneity, but the predictions of the configuration "iron in silver" is less bad for these materials than it was for MI materials.
- The intraphase heterogeneity is never well modeled by the GSCS, especially for high strain values and for the iron phase. The configuration "silver in iron" gives always worse predictions than the other one.

This paper is devoted to set out some developments of the GSCS which may improve these strain heterogeneity predictions, especially for MI materials. It gives also some conditions for the applicability of such a model. The final purpose of the study is the elaboration of a model capable of predicting the strain heterogeneities for different morphologies.

EXTENSIONS TO THE GENERALIZED SELF CONSISTENT SCHEME

Interpretation of the strain field in the composite inclusion

The analysis of elastic heterogeneous materials proposed by Stolz and Zaoui [5] suggests that the medium should be described as a set of inhomogeneous domains, representative of the microstructure. If these domains are isotropically distributed with respect to each other, the localization problem reduces to the resolution of several auxiliary problems consisting of these "morphologically representative patterns" embedded in an infinite medium. When this medium is chosen as weaker or harder than all phases of the material, the localization problem allows to derive bounds for the elastic properties of such materials. When it has the properties of the equivalent homogeneous medium, this approach generates a large class of self-consistent models, which give the effective behavior of materials in which these patterns are distributed in a "perfectly disordered" manner. This concept of perfect disorder has to be understood in the sense given by Kröner for the classical self-consistent model [6], where it applies to

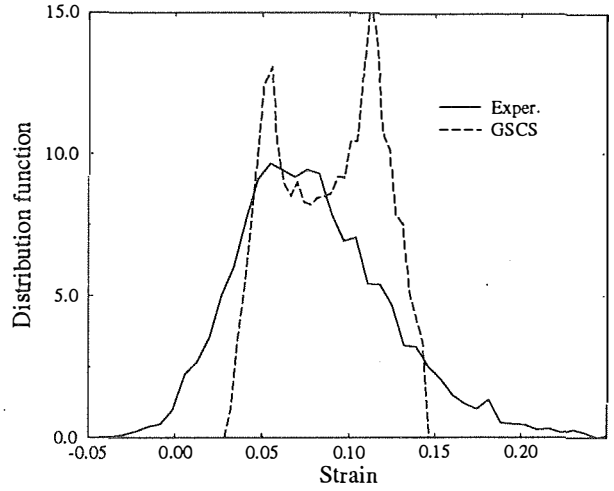

FIG 3. Strain distribution function in the silver at 5% global strain

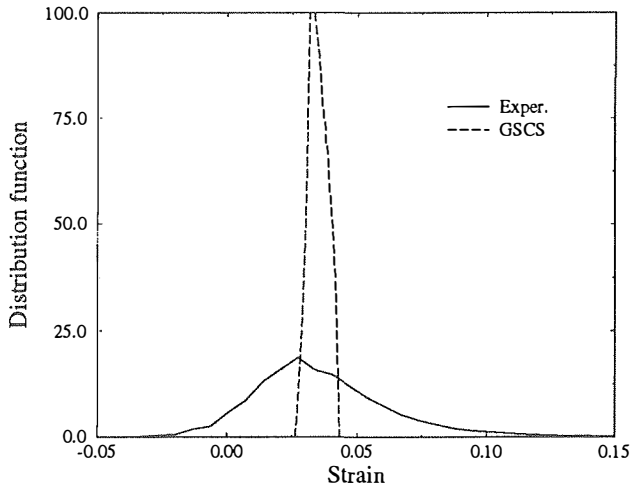

FIG 4. Strain distribution function in the iron at 5% global strain

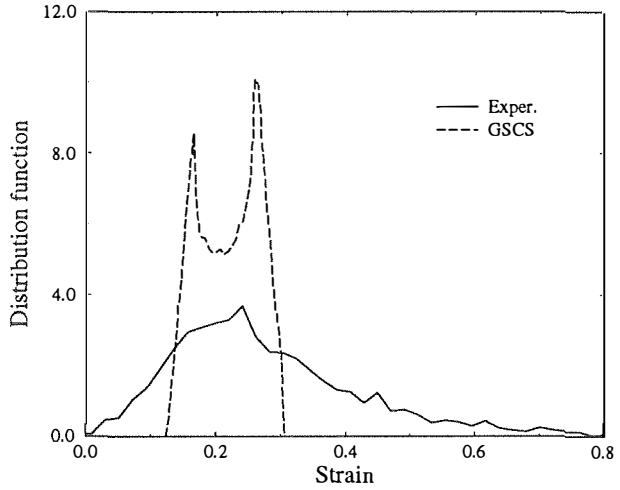

FIG 5. Strain distribution function in the silver at 15% global strain

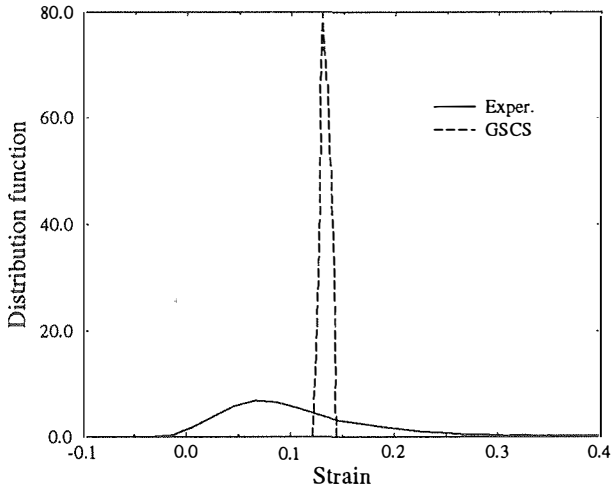

FIG 6. Strain distribution function in the iron at 15% global strain

the distribution of the mechanical phases. The concept of "perfectly disordered distribution of patterns" is defined by analogy with the punctual case, but is doesn't have a clear mathematical definition yet. The analysis shows also that the local strain computed in a pattern is the average of the local strain values in such a heterogeneous material, taken at all homologous points of this pattern.

Hervé et al. [7] have shown that the GSCS may be considered as a particular case of this general approach: there is only one pattern, the composite inclusion, defined as a spherical core of "inclusion phase" surrounded by a shell of "matrix phase" and with a volume fraction equal to the concentration of the material. Only one inclusion problem has then to be solved. This description of the material is appropriate for composites which clearly have a "matrix/inclusion" structure, with a perfectly disordered distribution of inclusions.

These analyses have only been established in the case of elasticity. We will nevertheless use their results in the elastoplastic case, which can be dealt with by such models when their elastic formulation is extended to nonlinear cases with use of secant moduli and an average strain-based condition of self-consistency, as shown by Hervé and Zaoui [4].

Modeling concentration fluctuations

Even if the "matrix/inclusion" pattern is an accurate representation of the MI materials in the elastic case, it might be too rough in the elastoplastic case, and this may explain the observed discrepancies between model and measurements.

The first extension proposed in the present work suggests that local concentration fluctuations could be responsible for the wider strain distribution. They may be modeled by two or even more different composite inclusions, with different volume fractions. The concentration of these "morphological phases" are chosen such that the global concentrations of the "mechanical phases" equal the global concentrations in the material. The localization problem reduces then to several composite inclusion problems, one for each local phase concentration, as shown in figure 7.

Modeling "morphological inversions"

It is also possible to model the microstructure as a mixture of both configurations of the composite inclusion, "iron in sil-

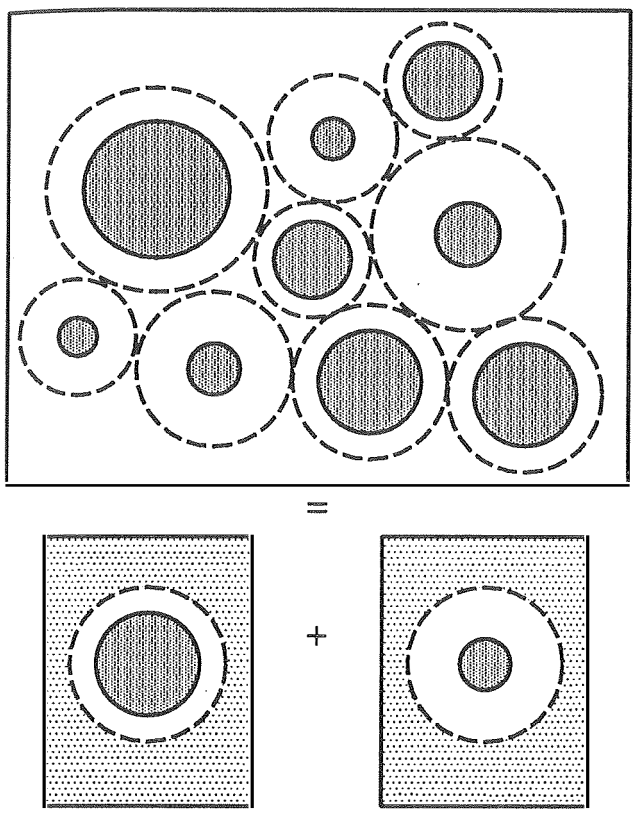

FIG 7. Modeling concentration fluctuations

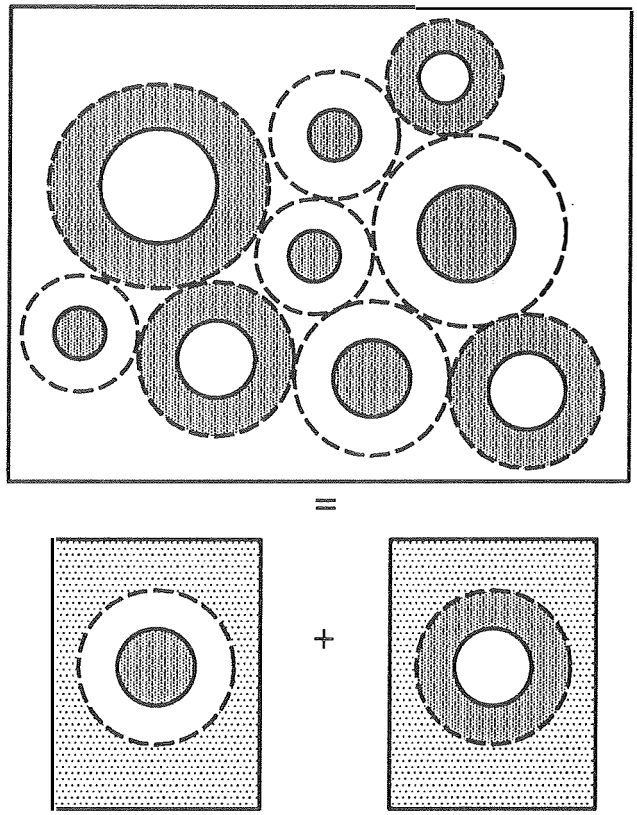

FIG 8. Modeling morphological inversions

ver" and "silver in iron", with identical or different volume fractions. This may describe local "morphological inversions": the matrix phase in a given composite material may locally be surrounded by the inclusion phase, and therefore behave as an inclusion. When the volume fractions of both configurations are close, this approach could also be a rough description of composite materials which have bi-continuous phases, in the sense that in this case both mechanical phases are partially surrounded by- and surrounding- the other phase. The localization problem leads then also to the resolution of several composite inclusion problems (see figure 8).

Improvement of the nonlinear extension

The results of Christensen and Lo [3], available for isotropic elasticity, have been extended to the nonlinear case by Hervé and Zaoui [4]. They used a deformation theory of plasticity, based on secant shear moduli. In this approach, the local stress is related to the local strain by the relations:

$$\begin{cases} \pi &= k\theta \\ \underline{\underline{s}} &= 2\mu^{sc}(\epsilon_{eq})\underline{\underline{e}} \end{cases} \qquad (1)$$

where $\pi\underline{\underline{1}}$ and $\underline{\underline{s}}$ are the isotropic and deviatoric parts of the stress, and $\theta/3\underline{\underline{1}}$ and $\underline{\underline{e}}$ are the isotropic and deviatoric parts of the strain. $\mu^{sc}(\epsilon_{eq})$ is the secant shear modulus, function of the equivalent strain ϵ_{eq} defined as:

$$\epsilon_{eq} = \sqrt{\frac{2}{3}\underline{\underline{e}} : \underline{\underline{e}}} \qquad (2)$$

The function μ^{sc} characterizes the plastic behavior of the material and can be identified in a uniaxial tensile test. These relations derive from a Hencky-Mises flow rule when the loading is proportional and monotonic. But since the local stress path in the composite inclusion is not proportional in the nonlinear case, they give only an approximate way to extend the elastic results to plasticity.

The second approximation made in [4] is that the shear modulus is supposed to be uniform in the kernel as well as in the shell, even if the strain field is not. The used shear modulus is the one associated with the equivalent mean strain of the shell or the kernel, for instance:

$$\mu_{shell} = \mu^{sc}_{shell}((< \underline{\underline{\epsilon}} >_{shell})_{eq}) \qquad (3)$$

where $< . >_{shell}$ means averaging over the shell. The obtained strain field, which is used to compute the strain distribution, is therefore the elastic strain field which corresponds to these moduli and may be different from the actual elastoplastic field generated in the composite material.

Radial discretization of the composite inclusion

To get a better approximation of this field, the composite sphere can be discretized into several concentric layers, each of them having its own secant modulus, associated with its equivalent average strain. This is possible thanks to the analytical solution of the multi-layered inclusion embedded in an infinite medium given by Hervé and Zaoui [8]. This allows to take into better account the strain gradient along the radius of the inclusion but still smoothes out the heterogeneity along the orthoradial directions.

New work-hardening parameter of a layer

An other possible modification of the nonlinear extension is to replace the definition (3) of the secant shear modulus of

the shell, the kernel or any layer l in case of a discretization, by the following one:

$$\mu_l = \mu_l^{sc}(< \epsilon_{eq} >_l) \tag{4}$$

This has been proposed first by Thébaud et al. [9] and modifies the work-hardening behavior of the layers since it takes into better account local heterogeneities which are smoothed out in the first definition. The problem in this approach is that there is no closed form expression for $< \epsilon_{eq} >_l$ and its calculation needs a time consuming numerical integration. Other definitions of μ_l are possible. We can suggest the following one:

$$(< \mu_l^{sc}(\epsilon_{eq}(.))\underline{\underline{\epsilon}}(.) >_l)_{eq} = \mu_l(< \underline{\underline{\epsilon}}(.) >_l)_{eq} \tag{5}$$

or its dual expression:

$$(< \underline{\underline{s}}(.)/\mu_l^{sc}(\sigma_{eq}(.)) >_l)_{eq} = (< \underline{\underline{s}}(.) >_l)_{eq}/\mu_l \tag{6}$$

These expressions define μ_l as a homogenized secant modulus over a layer, in a particular stress or strain approach, but they have not been tested.

Note that these remarks apply only for the layers in the composite inclusions. The behavior of the infinite medium in which they are embedded, has to be homogeneous in the sense of Hill's self-consistent approach for elastoplastic materials (Hill [10]). The secant shear modulus for the infinite medium is homogeneous and is the one associated to the equivalent strain at infinity according to the behavior of the infinite medium.

MATHEMATICAL FORMULATION AND RESOLUTION

This part will be devoted to the mathematical formulation and resolution of the problem of a micro-structure described as an assemblage of several morphologically representative patterns, each of them having the structure of a multi-layered inclusion.

Description of the assemblage

Consider (see figure 9) an assemblage of P patterns $p \in [1, P]$, each having L_p layers $l \in [1, L_p]$. The pure material in the layer l of the pattern p is $m_{pl} \in [1, M]$. In each composite inclusion, layer 1 is the central core and layer L_p is the external layer, surrounded by the infinite medium, which will be denoted by the subscript $_\infty$ and is made of material m_∞. The following notations will be used for the concentrations:

- C_p : concentration of the pattern p in the material;
- c_{pl}^p : concentration of the layer (p, l) in the pattern p;
- c_{pl} : concentration of the layer (p, l) in the material;
- γ_m : concentration of pure material m in the composite material;

The following relations are satisfied:

$$\left\{ \begin{array}{lcl} c_{pl} & = & C_p.c_{pl}^p \\ \gamma_m & = & \sum_{p,l|m_{pl}=m} c_{pl} \end{array} \right. \tag{7}$$

The M physical phases and the infinite medium are characterized by their constant bulk modulus k_m and their secant shear modulus function $\mu_m^{sc}(.)$. The materials in each layer then obey the nonlinear elastic isotropic law:

$$\left\{ \begin{array}{lcl} \pi & = & k_{pl}\theta \\ \underline{\underline{s}} & = & 2\mu_{pl}\underline{\underline{e}} \end{array} \right. \tag{8}$$

with

$$\left\{ \begin{array}{lcl} k_{pl} & = & k_{m_{pl}} \\ \mu_{pl} & = & \mu_{m_{pl}}^{sc}(E_{pl}) \end{array} \right. \tag{9}$$

where E_{pl} characterizes the work-hardening state of the layer and is defined by:

$$E_{pl} = (< \underline{\underline{\epsilon}} >_{pl})_{eq} \quad \text{or} \quad E_{pl} = < \epsilon_{eq} >_{pl} \tag{10}$$

Let $\underline{\underline{\epsilon}}_{pl}$ and $\underline{\underline{\sigma}}_{pl}$ denote the mean strain and mean stress tensors in the layer (p, l); $\underline{\underline{\epsilon}}_\infty$ and $\underline{\underline{\sigma}}_\infty$ are the homogeneous strain and stress tensors applied at infinity. All of them may be decomposed into their isotropic and deviatoric parts, with the same notations than previously. The work-hardening parameter of the infinite medium is $E_\infty = (\underline{\underline{\epsilon}}_\infty)_{eq}$. We also define the subscript $_0$ which denotes the mean value over all patterns for the stress or the strain tensors:

$$\left\{ \begin{array}{lcl} \underline{\underline{\epsilon}}_0 = & < \underline{\underline{\epsilon}} > & = \sum_{p,l} c_{pl}\underline{\underline{\epsilon}}_{pl} \\ \underline{\underline{\sigma}}_0 = & < \underline{\underline{\sigma}} > & = \sum_{p,l} c_{pl}\underline{\underline{\sigma}}_{pl} \end{array} \right. \tag{11}$$

This allows to define the moduli k_0 and μ_0 such that:

$$\left\{ \begin{array}{lcl} \pi_0 & = & k_0\theta_0 \\ \underline{\underline{s}}_0 & = & 2\mu_0\underline{\underline{e}}_0 \end{array} \right. \tag{12}$$

as well as a mean work-hardening parameter $E_0 = (\underline{\underline{\epsilon}}_0)_{eq}$. Note that the definition of μ_0 assumes proportionality between $\underline{\underline{s}}_0$ and $\underline{\underline{e}}_0$ which will be checked later on.

Computation of the mechanical state of the assemblage

Let us first suppose that the behavior of all pure materials and of the infinite medium are known. The problem is then to find the "state" of the assemblage, that means the local stress and strain states in all patterns, when a uniaxial tension is applied at infinity, and when E_{pl} for a given layer (p, l) or E_∞ or E_0 is prescribed. When all secant moduli are known, the displacement field in each composite inclusion can be computed as a function of the strain at infinity, thanks to the relations given in [8]. Their derivation gives the local strain field and, after averaging, all the work-hardening parameters. These are positively homogeneous functions of degree one of the strain at infinity, so that the latter may be rescaled in order to obtain the imposed work-hardening value and all other corresponding work-hardening parameters. These allow to recompute the secant moduli for all layers according to their known behavior. The solution is reached when the obtained moduli equal the initially used ones. The resolution of this nonlinear problem has been achieved thanks to an iterative algorithm which is described in the appendix. Once the solution is reached, it is easy to compute the local stress values.

Self-consistent approach

In a generalized self-consistent approach, the infinite medium has the characteristics of the equivalent homogeneous medium. The condition of self-consistency which has been used is based on the mean strain condition:

$$\underline{\underline{\epsilon}}_0 = \underline{\underline{\epsilon}}_\infty \tag{13}$$

In the case of the classical elastic GSCS, this condition is equivalent to the energy based condition used by Christensen

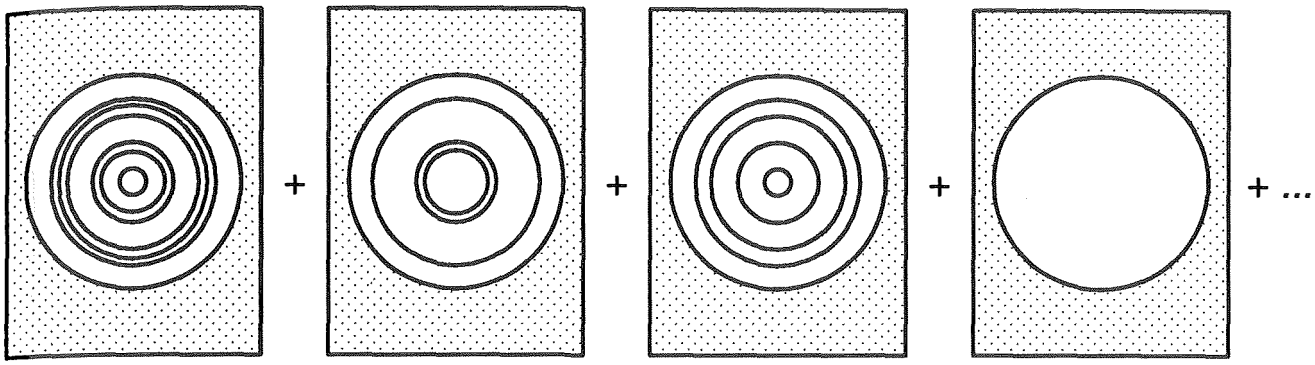

FIG 9. P patterns of type "n-phase"

and Lo [3] as shown by Hervé and Zaoui [4]. It is also equivalent to the condition (see [4])

$$\left\{ \begin{array}{rcl} \mu_o & = & \mu_\infty \\ k_o & = & k_\infty \end{array} \right. \tag{14}$$

which has been used in this work. When this condition is satisfied, k_o and μ_o are equal to the bulk and shear moduli of the equivalent homogeneous medium $k_\star$ and $\mu_\star$ corresponding to the work-hardening parameter E_o, which then equals E_∞.

The solution of the n-layered inclusion given in [8] shows that the deviatoric part of the mean strain in a layer is proportional to the deviatoric part of the strain at infinity:

$$\underline{\underline{e}}_{pl} = a_{pl} \underline{\underline{e}}_\infty \tag{15}$$

The scalar a_{pl} has a closed form which is given in [8] :

$$a_{pl} = a_{pl}(\{c^p_{pk}, \mu_{pk}, k_{pk}, 1 \leq k \leq L_p\}, \mu_\infty, k_\infty) \tag{16}$$

The deviatoric part of the mean stress in a layer is given by:

$$\underline{\underline{s}}_{pl} = 2\mu_{pl} \underline{\underline{e}}_{pl} = 2\mu_{pl} a_{pl} \underline{\underline{e}}_\infty \tag{17}$$

The mean deviatoric strain and stresses are thus:

$$\left\{ \begin{array}{rcl} \underline{\underline{e}}_o & = & (\sum_{p,l} c_{pl} a_{pl}) \underline{\underline{e}}_\infty \\ \underline{\underline{s}}_o & = & 2(\sum_{p,l} c_{pl} a_{pl} \mu_{pl}) \underline{\underline{e}}_\infty \end{array} \right. \tag{18}$$

They are proportional as previously mentioned. This finally gives:

$$\mu_o = \frac{\sum_{p,l} c_{pl} a_{pl} \mu_{pl}}{\sum_{p,l} c_{pl} a_{pl}} \tag{19}$$

The same relation can be derived for the isotropic part:

$$\theta_{pl} = b_{pl} \theta_\infty \tag{20}$$

with (see [8]):

$$b_{pl} = b_{pl}(\{c^p_{pk}, \mu_{pk}, k_{pk}, 1 \leq k \leq L_p\}, \mu_\infty, k_\infty) \tag{21}$$

$$k_o = \frac{\sum_{p,l} c_{pl} b_{pl} k_{pl}}{\sum_{p,l} c_{pl} b_{pl}} \tag{22}$$

The computation of $\mu_\star$ and $k_\star$ for a given value of E_∞ uses the non-linear iterative procedure described in the appendix; the state of the assemblage has to be computed in each iteration, so that this algorithm has two levels of iteration. The complete $\mu^{sc}_\star$ function may be computed piecewise when this procedure is reproduced for several values of E_∞.

Note that in this approach, $k_\star$ is not constant: the plastic flow of the equivalent homogeneous medium is not incompressible; nevertheless, the dependence remains very weak in the tested cases and can be neglected.

This algorithm may be generalized: it is possible, with the same formulation, to compute the behavior of the material in a given layer when the behavior of the equivalent homogeneous medium and the behavior of the pure materials in all the other layers are known. That's what has in fact been done in the case of the materials considered here. For metallurgical reasons, the local behavior of iron in the two-phase materials was not identical to the behavior in the pure iron samples, as shown by micro-hardness tests (see [1]). The actual behavior of the iron in each blend has thus been computed according to the classical GSCS, with help of the macroscopic tensile test curve of the blend and the pure silver phase (whose behavior does not vary from one sample to the other). Since the macroscopic behavior is not very sensitive to the configuration of the GSCS, this procedure gives the tensile test curve of the iron phase in the two-phase material accurately enough. The obtained curve can then be used for the computation of strain heterogeneities according to the same configuration of the GSCS or to any other "multi-patterned" and "multi-layered" configuration of the above described extension.

Computation of strain distribution functions

In order to obtain the strain distribution function in each phase according to a given configuration of the extended GSCS and at a given macroscopic strain, one has to compute firstly the macroscopic behavior of the sample, then to compute the state of the assemblage which corresponds to the prescribed macroscopic strain. The composite inclusions of the assemblage are then discretized along their radius and their polar angle. The considered strain component, usually the component along the tensile axis, is computed at the center of the obtained elements. The extremal values for each phase are determined and the obtained intervals are discretized into several classes of the same width. These are weighted by the global volume fraction of the elements whose strain value belongs to them (the global volume fraction is obtained as the product of the local volume fraction of the element in the pattern by the global volume fraction of the pattern). The value of the strain distribution function at the center of each class

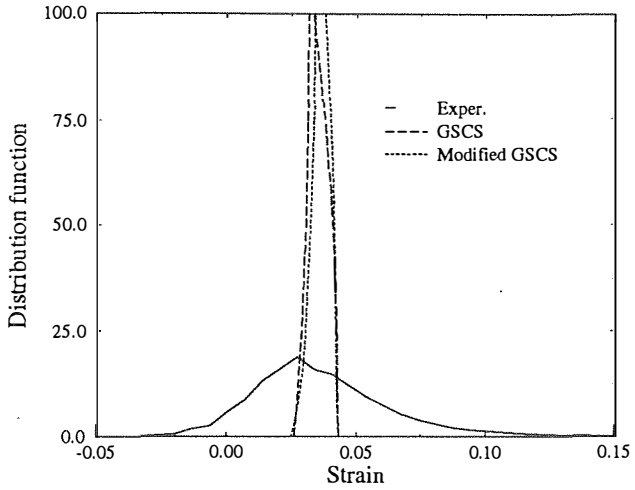

FIG 10. Concentration fluctuation (iron at 5% global strain)

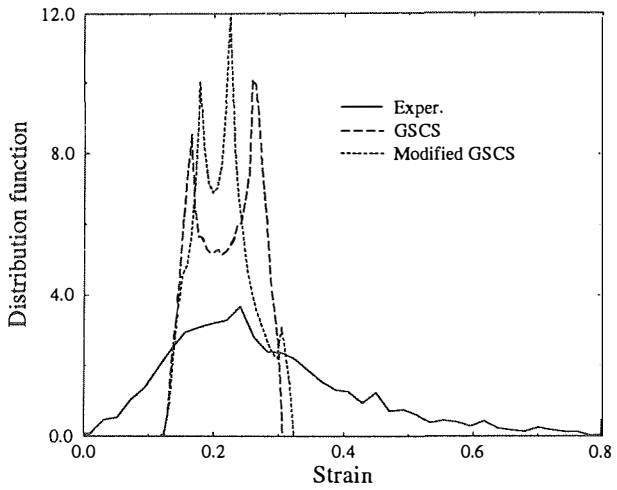

FIG 11. Concentration fluctuation (silver at 15% global strain)

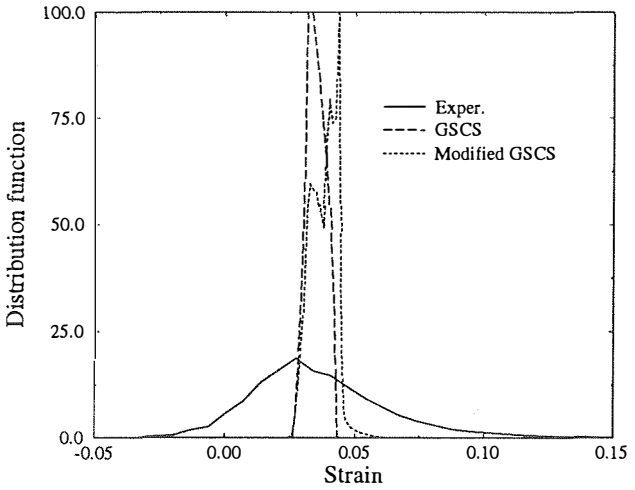

FIG 12. Morphological inversion (iron at 5% global strain)

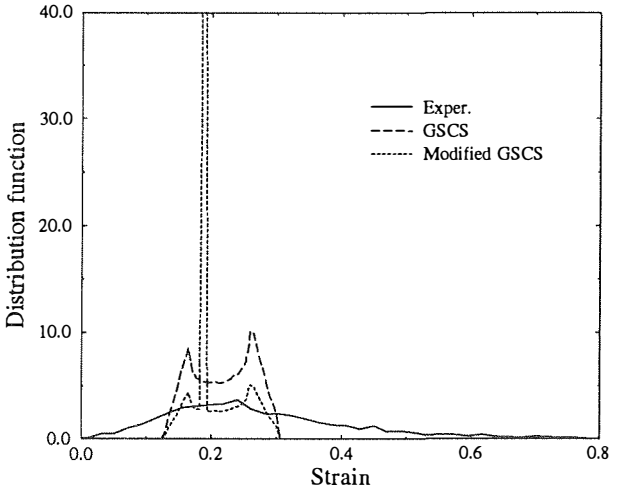

FIG 13. Morphological inversion (silver at 15% global strain)

is then defined as the weight of this class, after normalization. Since analytical expressions of the strain field are used, it is possible to use very fine discretizations: each composite inclusion may be cut into 10000 or even more elements. About 50 classes are used for the piecewise construction of the distribution function.

There is no theoretical limitation to the number of patterns or layers. Since these computations are based on analytical relations, they are not very power consuming when the first definition of the work-hardening parameters is used. Models with about 50 internal parameters (i.e. 50 layers spread out over several patterns) can be computed on a personal computer. The second definition needs a numerical integration, which is usually performed with about 100 integration points in each layer. This computation can easily be achieved on a workstation.

RESULTS

Effect of concentration fluctuations

When several patterns are used, the local concentration of each pattern can be chosen arbitrarily. Figure 10 and 11 show the strain distribution obtained with two patterns of type "iron in silver"; the first one has 67% iron and its volume fraction is 40%; the second one has 92% iron and its volume fraction is 60%, so as to respect the global iron concentration of 82%. One can observe that the strain distribution is almost unchanged in iron. It looks somewhat different in the silver phase but its width is also quite the same. Other combinations of patterns have also been tested, but none of them gives larger heterogeneities. It is possible to compute large strain values when patterns with a very thin silver shell are used. But since the volume of such shells may be neglected in comparison to the global volume of the phase, the resulting strain distribution is narrower than the one shown here. The interphase heterogeneity is slightly reduced in comparison to the results of the GSCS.

Effect of morphological inversions

Figure 12 and 13 give the strain distribution obtained with two patterns which have the same local concentration (82% iron) and are present in the same proportions, but with opposite morphologies. The strain distribution in iron is slightly enlarged, as a result of the peripheral position of half of the iron content. The extremal strain values computed in the

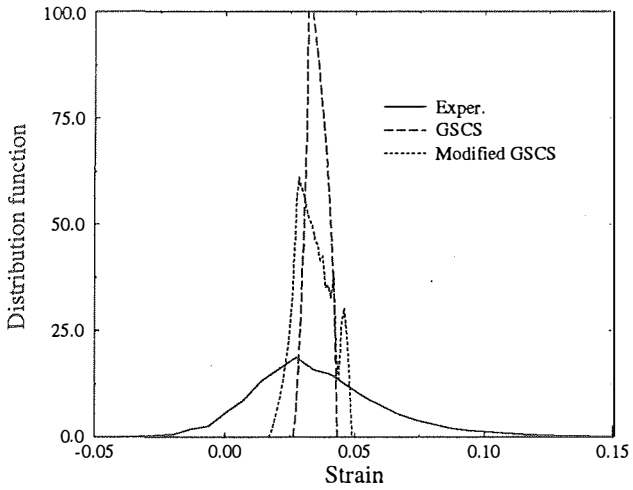

FIG 14. New non-linear extension (iron at 5% global strain)

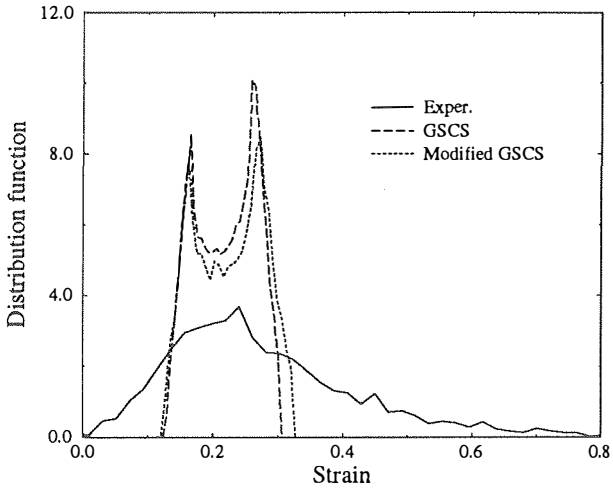

FIG 15. New non-linear extension (silver at 15% global strain)

silver phase are unchanged, but the distribution width is reduced since silver in the core is quite homogeneously strained. The resulting average strains per phases lay between the values obtained with the opposite configurations of the GSCS.

Effect of the improvement of the nonlinear extension

The improvement of the nonlinear extension has been experimented on the single pattern "iron in silver": both the core and the shell have been discretized into ten layers of the same volume and relation 4 has been used for the characterization of the work-hardening state of a layer. $< \epsilon_{eq} >_{layer}$ has been integrated numerically with 2 integration points along the radius and 30 along the polar angle in each layer. One can observe that this modification has only a tiny effect on the strain distribution in the shell. It enlarges the heterogeneity in the core, but the resulting heterogeneity is still too narrow in comparison to the experimental one. The interphase heterogeneity is slightly enlarged but much too slightly to fit the experimental results.

It is possible to combine all these modifications in a unique computation; this improves slightly the strain heterogeneity predictions of the GSCS, but not enough to be really representative of the experimental results.

It is also possible to test these modifications on BC materials, but the conclusions are almost the same. The elastic constants that are obtained with two patterns of same local concentration but with opposite configurations, designed to simulate roughly structures with bi-continuous phases, are consistent with the experimental measures: the obtained values are intermediate between these obtained with the two opposite configurations of the GSCS. But in the elastoplastic case, the computed strain distributions are similar to those obtained for MI materials, and very different from the experimental results.

NUMERICAL MODELING

Since no basic difference was found between the computation of the elastoplastic strain field in the classical GSCS and in the layer-discretized inclusion, one can suppose that the heterogeneity is due to strain gradients along orthoradial directions, which cannot be computed correctly in an analytical form. That's why the elastoplastic composite inclusion problem has been solved numerically with help of classical finite elements techniques. Figure 18 shows the mesh: an axisymmetric four-noded bilinear element with four integration points has been used within a small deformation formulation. The extension of the infinite medium has been limited to three times the radius of the inclusion and tractions have been applied to the boundary of the mesh, in order to simulate a macroscopic homogeneous uniaxial tensile stress state. This extension of the infinite medium seems to be sufficient since an almost homogeneous strain state has been obtained at the boundary. A von Mises elastoplastic criterion has been combined to normal flow rule and isotropic work-hardening. The work-hardening curve of the infinite medium is the one computed with the classical GSCS. Note that this problem does not conform exactly to the self-consistent formulation, but should nevertheless give a satisfying approximation of the strain field in the inclusion.

Figures 19, 16 and 17 compare the numerical results to the analytical ones obtained with the classical GSCS. Both approaches differ slightly: in particular the strain distribution function obtained numerically fits better the experimental distribution in silver for low strain values. But the distribution still remains too narrow in comparison to the experimental results in all other cases.

These numerical results prove that the discrepancy between experimental results and computations with the GSCS are not due to the approximate nonlinear extension of the elastic GSCS. In fact the deformation theory for elastoplasticity as presented in [4] gives satisfying informations with only short computations: the strain distribution function is obtained within a few seconds with the GSCS whereas several hours are needed on the same computer with the numerical approach.

ACTUAL STRAIN LOCALIZATION MODES

The device that has been used to measure experimentally the strain heterogeneity gives the local strain on points on a regular grid that covers a domain representative of the microstructure. This information allows to plot a strain map over this domain, which gives the actual localization of the strain (see [11]). Figure 20 gives the map that corresponds to an MI ma-

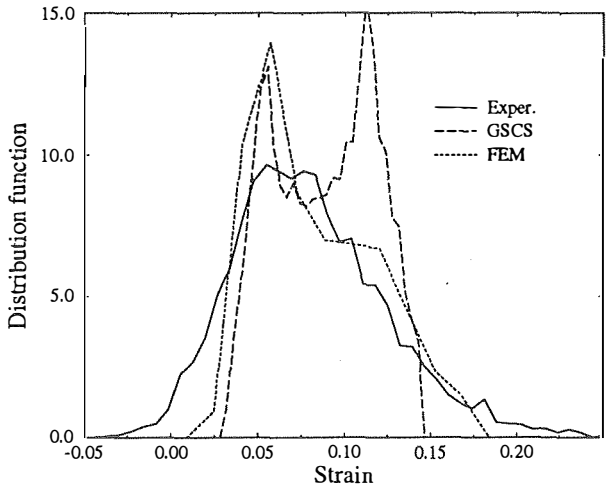

FIG 16. FEM results (silver at 5% global strain)

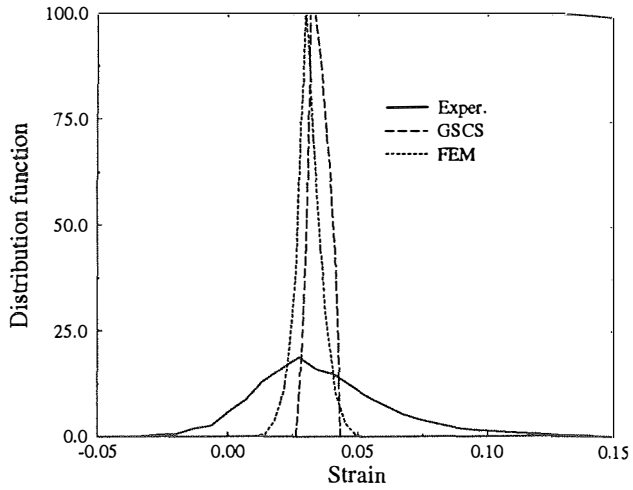

FIG 17. FEM results (iron at 5% global strain)

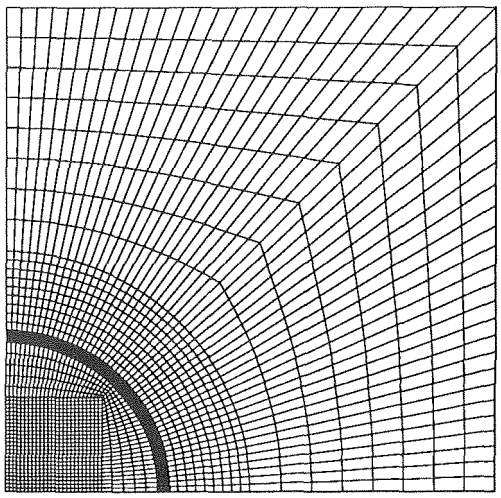

FIG 18. Mesh (2275 elements)

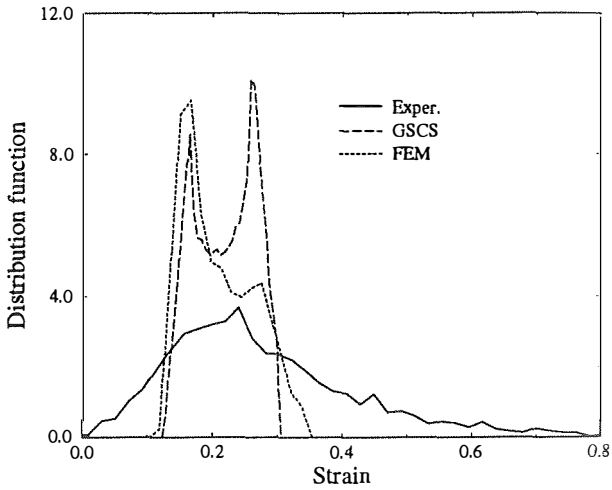

FIG 19. FEM results (silver at 15% global strain)

terial, with approximately 70% iron, at a macroscopic strain close to 10%. One can see that the strain basically localizes into long range shear bands that go through the weak silver phase, and sometimes "cut" locally the other phase. Such features certainly cannot be modeled by a self-consistent approach, which only takes into account local interactions and replaces all long range effects by their average. They could possibly be modeled if the sizes of the used patterns were larger than the characteristic length of such shear bands, provided that such a length exists. But such an approach cannot be achieved for practical reasons: at this time nobody is able to compute this kind of three-dimensional structures. These shear bands tend to enlarge the strain heterogeneity, especially in the weak phase where they appear and this may explain why the GSCS fails to predict the actual strain heterogeneity.

The heterogeneity in the harder phase may be explained by the local crossing of the shear bands mentioned above, but also by a shape effect that has not been taken into account in the GSCS: the spherical core of the composite inclusion is loaded almost like Eshelby's inclusion and thus quite homogeneously strained, especially when its volume fraction is small. The iron inclusions in the MI structures have much more complex shapes; to replace them by spheres leads certainly to neglect much of their morphological particularities. These shape parameters have probably only local effects which could be estimated by a self-consistent approach. But this requires to design patterns representative of these morphological parameters and to compute them, which has not yet been solved.

These long range shear bands have not been observed on BC materials, or their characteristic length was much smaller. This is probably due to the fact that in these materials such bands would have to shear much more harder phase to cross continuously the microstructure than in MI materials, and thus are at a disadvantage on an energetical point of view. The strain localization mode remains local. This explains why the strain field is less heterogeneous in these materials and why the predictions of the GSCS are better for them, even if this model is not designed for BC microstructures.

CONCLUSIONS

The aim of this paper was to suggest some extensions to the Generalized Self Consistent Scheme in order to use the local fields computed in the composite inclusion as predictions

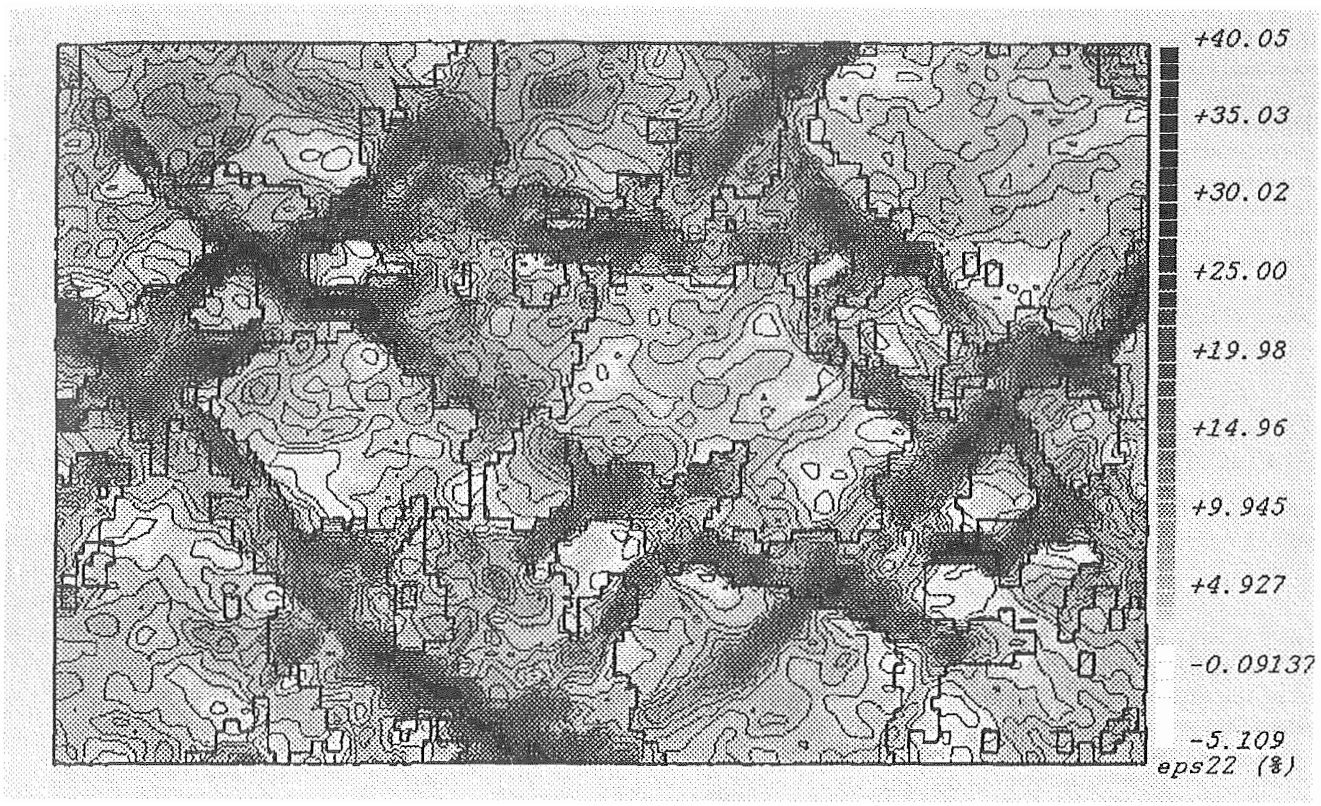

FIG 20. Strain map over a representative domain of an MI microstructure (the interface is bold and the tensile axis is vertical)

of the strain distribution in two-phase elastoplastic materials. It has been shown how it is possible to model morphological situations which are more general than the classical "perfectly disordered" matrix/inclusion structure: in particular local concentration fluctuations and local morphological inversions have been described. These approaches are based on a rigorous theoretical analysis of elastic heterogeneous materials and are extended to elastoplasticity by means of the deformation theory and the use of secant moduli.

Unfortunately these extensions are not sufficient to model the elastoplastic strain heterogeneities measured experimentally on iron/silver blends, whose microstructures are close to a matrix/inclusion microstructure. The discrepancy is not due to the approximate computation of the elastoplastic strain field in the composite inclusion, since several extensions, including discretization of the composite inclusion, modification of the work-hardening parameters of the phases or numerical computation based on finite element techniques give quite the same result. In fact the approximate deformation theory of elastoplasticity gives almost the same informations than more elaborated techniques, but with much shorter computations.

The discrepancy between the measured distribution of strain in the weak matrix phase and computation results is related to the localization of the strain into long range shear bands. These bands cannot be modeled by self-consistent approaches which basically take only into account local and average interactions. The width of the strain distribution in the harder inclusion phase is also strongly underestimated. This is probably due to the inability of a spherical inclusion to represent the true morphology of the inclusions in the material. The definition of more representative patterns combined to a self-consistent approach should allow to get a better estimation of these strain heterogeneities. But how to define these "morphologically representative patterns" and how to compute them are still open questions.

REFERENCES

1. Allais L, Effet de la morphologie et de la répartition spatiale des phases sur le comportement mécanique des materiaux biphasés, PhD Thesis, Université Paris XIII, 1991.
2. Allais L, Bretheau T, and Hervé E, Phase morphology and plastic behaviour of two-phase materials, in *Proceedings of the 7th Symposium on Continuous Models and Discret Systems*, Paderborn, 1992.
3. Christensen RM and Lo KH, Solution for effective shear properties in three phase sphere and cylinder models, *Journal of the Mechanics and Physics of Solids*, 27, 315–330 (1979).
4. Hervé E and Zaoui A, Modeling the effective behavior of nonlinear matrix inclusion composites, *European Journal of Mechanics A/Solids*, 9(6), 505–515 (1990).
5. Stolz C and Zaoui A, Analyse morphologique et approches variationnelles du comportement d'un milieu élastique hétérogène, *Compte-rendus à l'Académie des Sciences*, II(312), 143–150 (1991).
6. Kröner E, Graded and perfect disorder in random media elasticity. *Journal of the Engineering Mechanics Division*, 106(EM5), 889–914 (1980).
7. Hervé E, Stolz C, and Zaoui A, A propos de l'assemblage des sphères composites de Hashin, *Compte-rendus à l'Académie des*

Sciences, II(313),857–862 (1991).

8. Hervé E and Zaoui A, N-layered inclusion-based micromechanical modeling. *International Journal for Engineering Sciences*, 31(1), 1–10 (1993).
9. Thébaud F, Michel JC, Hervé E, Suquet P, and Zaoui A, Modeling nonlinear behavior of composites with imperfect interfaces, in *Proceedings of the 13th Risø International Symposium on Materials Science*, SI Andersen (ed), 1992, 467–472.
10. Hill R, Continuum micro-mechanics of elastoplastic polycrystals, *Journal of the Mechanics and Physics of Solids*, 13, 89–101 (1965).
11. Allais A, Bornert M, Caldemaison D, and Bretheau T, to be published (1993).

ALGORITHM FOR NONLINEAR EQUATIONS

The nonlinear problems to be solved in this work can all be written in a same symbolic form:

$$U = F(U, P)$$

where U are the unknowns and P the parameters of the problem. F is nonlinear in U. In case of the computation of the state of the assemblage, U is the set of work-hardening parameters (or secant moduli) of the layers. U is the couple $(k_\star, \mu_\star)$ in the case of the self-consistent computation of the equivalent homogeneous medium.

The fixed-point algorithm is most of the time unstable. The following more elaborated algorithm has been used. Let $N(U)$ characterize the distance to the solution:

$$N(U) = \| U - F(U, P) \|$$

where $\| \cdot \|$ is any norm (usually the Euclidian norm). The solution is such that $N(U) = 0$. The iterative procedure begins with any value of U. U_{n+1} is computed from U_n according to following relations:

$$U_{n+1} = U_n + \lambda_n (F(U_n, P) - U_n)$$

with λ_n chosen such that:

$$N(U_n) + \lambda_n p_n = 0$$

with

$$p_n = \frac{dN}{dU}(U_n).(F(U_n, P) - U_n)$$

p_n is computed numerically by

$$p_n = \frac{N(U_n + \gamma(F(U_n, P) - U_n)) - N(U_n)}{\gamma}$$

where γ is a coefficient close to zero (usually 1%). The iteration is stopped when $N(U)/\| U \|$ is less than the desired precision (10^{-7} is a usual value). This algorithm is a mixture of the fixed-point algorithm and a gradient algorithm. It proves stable and easy to implement.